Comparative Medicine
Copyright 2003
by the American Association for Laboratory Animal Science

Vol 53, No 2
April 2003
Pages 197-206

Pathogenesis of Mouse Hepatitis Virus Infection in Gamma Interferon-Deficient Mice Is Modulated by Co-infection with *Helicobacter hepaticus*

Susan R. Compton, PhD,* Lisa J. Ball-Goodrich, PhD, Caroline J. Zeiss, BVSc, PhD, Linda K. Johnson, DVM, Elizabeth A. Johnson, and James D. Macy, DVM

Gamma interferon-deficient (IFN-γ KO) mice developed a wasting syndrome and were found to be co-infected with *Helicobacter* sp., and a new isolate of mouse hepatitis virus (MHV) designated MHV-G. The disease was characterized by pleuritis, peritonitis, hepatitis, pneumonia, and meningitis. Initial experiments used a cecal homogenate inoculum from the clinical cases that contained *H. hepaticus* and MHV-G to reproduce the development of peritonitis and pleuritis in IFN-γ KO mice. In contrast, immunocompetent mice given the same inoculum developed an acute, self-limiting infection and remained clinically normal. This result confirmed the importance of IFN-γ in preventing chronic infection and limiting viral dissemination. To understand the role of both agents in the development of peritonitis and pleuritis, IFN-γ KO mice were infected with either agent or were co-infected with *H. hepaticus* and MHV-G. Infection with MHV-G induced a multisystemic infection similar to that described in the original cases, with multifocal hepatic necrosis, acute necrotizing and inflammatory lesions of the gastrointestinal tract, and acute peritonitis and pleuritis with adhesions on the serosal surfaces of the viscera. However, mice given *H. hepaticus* alone had minimal pathologic changes even though the organism was consistently detected in the cecum or feces. Although co-infection with *H. hepaticus* and MHV-G induced lesions similar to those associated with MHV-G alone, the pathogenesis of the MHV infection was modified. *Helicobacter hepaticus* appeared to reduce the severity of MHV-induced lesions during the acute phase of infection, and exacerbated hepatitis and meningitis at the later time point. We conclude that infection of IFN-γ KO mice with MHV-G results in multisystemic infection with peritonitis, pleuritis, and adhesions due to the aberrant immune response in these mice. In addition, co-infection of these mice with *H. hepaticus* results in alterations in the pathogenesis of MHV-G infection.

Mouse hepatitis virus (MHV) is a singular name for a group of murine coronaviruses that cause a wide spectrum of clinical outcomes ranging from subclinical infection to enteritis, hepatitis, and encephalitis. Enterotropic MHV strains, such as MHV-Y, initially replicate in epithelial cells of the gastrointestinal (GI) tract after infection of adult immunocompetent mice. Disease is acute and mild with minimal pathologic changes, and virus rarely disseminates to other organs (1-3). In contrast, morbidity and mortality are high in neonatal immunocompetent mice, and infection of immunocompromised mice can cause multisystemic, persistent infection with extended viral shedding (4) and high mortality (5). Polytropic MHV strains, such as MHV-A59 or MHV-JHM, initially replicate in the proximal respiratory tract epithelium after infection, then disseminate to many organs via viremia, lymphatic spread, or olfactory pathways from the nose to the brain. Infection of adult immunocompetent mice results in subclinical infection, hepatitis, and/or encephalitis (6), whereas infection of immunocompromised mice can cause severe disseminated disease with high mortality.

Mouse hepatitis virus is the most prevalent viral pathogen in laboratory mouse colonies, and infections with enterotropic strains outnumber those with polytropic strains (7, 8). Increased incidence of MHV in mouse populations may be due, in part, to widespread use and exchange of unique, genetically altered mouse strains among universities and commercial establishments. In addition, many of these mouse strains are immunocompromised and MHV infection in these mice may be more severe or chronic, or may be associated with unexpected pathologic changes.

One genetically engineered mouse strain, in which viral and bacterial infections are more severe, is the gamma interferon (IFN-γ)-deficient mouse. Gamma interferon is an important cytokine in defense against microbial infections and an important regulator of the immune response (9). Gamma interferon knockout (KO) mice inoculated with *Klebsiella pneumoniae* or *Legionella pneumophila* had increased pulmonary bacterial load and increased mortality, as compared with immunocompetent mice (10, 11). Herpes simplex virus type-1 infection of mice deficient in IFN-γ progressed to skin and brain lesions, the severity of which exceeded those seen in immunocompetent mice (12). After infection with lymphocytic choriomeningitis virus, IFN-γ KO mice became chronically infected, although immunocompetent mice rapidly cleared the infection (13). Mouse hepatitis virus infection also has been reported in IFN-γ KO mice. A recent case report indicated that natural infection of C57BL/6 IFN-γ KO mice with MHV resulted in unexpected pathologic

Received: 11/20/02. Revision requested: 1/03/03. Accepted: 1/21/03.
Section of Comparative Medicine, Yale University School of Medicine, P.O. Box 208016, New Haven Connecticut 06520-8016.
**Corresponding author.*

changes, including extensive pleuritis and peritonitis (14). Additional evidence from experimental studies suggests that polytropic MHV infection also is altered in IFN-γ KO mice. Infection of C57BL/6 mice deficient in IFN-γ with MHV-JHM resulted in fatal peritonitis (15), while infection of BALB/c mice deficient in IFN-γ with MHV-JHM resulted in acute hepatic failure (16). Infection with MHV-A59 of 129 mice deficient in the IFN-γ receptor resulted in more severe hepatitis than did MHV-A59 infection in 129 wild-type mice (17). However, to the authors' knowledge, the pathogenesis of experimentally induced enterotropic MHV infection in IFN-γ KO mice has not been evaluated.

Helicobacters are the most prevalent bacterial pathogens in laboratory mice (7), and until recently, most academic and commercial mouse colonies were enzootically infected with them. Helicobacters are gram-negative, helical, microaerophilic bacteria. *Helicobacter hepaticus*, a urease-positive species, colonizes the cecum and colon and spreads to the liver of mice during chronic infection. *Helicobacter hepaticus* has been reported to cause enterocolitis and chronic proliferative hepatitis in immunocompetent mice (18), and causes inflammatory bowel disease in scid, nude, and several genetically altered mouse strains (19-22). Susceptibility to *H. hepaticus*-induced hepatitis has a genetic component. For example, A/J mice infected with *H. hepaticus* develop hepatitis, whereas C57BL/6 mice do not develop hepatitis (23). Conversely, A/J mice infected with *H. hepaticus* have lower long-term cecal colonization levels, compared with C57BL/6 mice (24). A Th1-type cytokine response, including induction of IFN-γ, has been associated with development of *H. hepaticus*-induced hepatitis (25) and inflammatory bowel disease (26-28). Additionally, production of IFN-γ is a factor in induction of gastric inflammation by *H. pylori* in immunocompetent mice; C57BL/6 IFN-γ KO mice did not manifest signs of inflammation (29).

We report findings from a clinical case in which C3H IFN-γ KO mice presented with diarrhea, dehydration, hunched posture, and dyspnea; histologic examination indicated that mice had peritonitis, pleuritis, and hepatic necrosis. Serologic and molecular analyses indicated that mice were co-infected with MHV and *Helicobacter sp.*. Because MHV and *Helicobacter* species replicate in and colonize a similar region of the GI tract, each may influence the infectivity and severity of disease caused by the other agent. Although, the impact of co-infections of *Helicobacter* sp. and enterotropic MHV is unknown, initial MHV-Y pathogenesis studies used intestinal virus stocks that were *Helicobacter* DNA positive based on polymerase chain reaction (PCR) analysis (2, 3). Infections were experimentally induced to confirm and elucidate the role(s) of MHV, *Helicobacter hepaticus*, and mouse genotype in the disease associated with the clinical cases.

Materials and Methods

Animals. The C3H IFN-γ KO (C3H-*Ifng*) mice were imported from a non-commercial academic source and were seronegative for ectromelia virus, lymphocytic choriomeningitis virus, minute virus of mice, mouse parvovirus, murine rotavirus, pneumonia virus of mice, reovirus, Sendai virus, and *Mycoplasma pulmonis*. Experimental studies used four- to six-week-old female BALB/cJ, Cby.Cg-*Foxn1*^{nu} (nude),and C.129S7(B6)-*Ifng*^{tm1Ts} (IFN-γ KO) mice (Jackson Laboratories, Bar Harbor, Maine) that were seronegative for mouse hepatitis virus, ectromelia virus, lymphocytic choriomeningitis virus, minute virus of mice, mouse parvovirus, murine rotavirus, pneumonia virus of mice, reovirus, Sendai virus, and *Mycoplasma pulmonis* , and were free of bacterial and parasitic infections on arrival. Colony sentinel mice were routinely tested for the parasites and were found free of endoparasitic and exoparasitic infections. All animal procedures were approved by the Yale Animal Care and Use Committee and animal care was in accordance with the NIH *Guide for the Care and Use of Laboratory Animals*.

Mice were housed in a quarantine facility, and room conditions included a negative pressure differential relative to the corridor, a 12:12-h light:dark cycle, and 10 to 15 air changes/h. Mice were housed on sterilized corncob bedding in sterilized cages (Polysulfone Standard Mouse Cage, Allentown Caging Equipment Co., Allentown, Pa.) equipped with stainless steel wire bar tops and filtered cage tops containing Reemay filter media (No. 2295, Allentown Caging Equipment Co.). Mice were fed sterilized standard rodent chow (Purina Mills, 5010, PMI, St. Louis, Mo.) and hyperchlorinated water ad libitum, using a water bottle. Cages were husbanded every seven days in a class-II biosafety cabinet in the animal room. The surfaces of the forceps and biosafety cabinet were decontaminated for a minimum of 60 sec between cages, using a 1:18:1 dilution of chlorine dioxide (Clidox, Pharmacal, Naugatuck, Conn.) prepared daily.

Viral and bacterial stocks. A 5% cecal homogenate from a C3H-*Ifng* clinically ill mouse 47 days after arrival that contained MHV-G (a new strain of MHV) and *H. hepaticus*, was used as inoculum in the first experimental infection. A 5% liver homogenate from an experimentally infected nude mouse 22 days after inoculation was collected during the first experimental infection and was used as inoculum for the second experiment. Anaylsis by PCR confirmed that the homogenate contained MHV-G, but not *Helicobacter* sp. *Helicobacter hepaticus* (a gift from Dr. Nirah Shomer) was cultured in Brucella broth supplemented with 5% fetal bovine serum, or on blood agar plates for three to five days in an 80% N_2, 10% CO_2, and 10% H_2 environment at 37°C. Bacteria were centrifuged for 15 min at 12,000 ×*g*, resuspended in Brucella broth to yield a dose equivalent to 10^7 colony-forming units /20 µl, and visualized by use of phase microscopy and Gram staining for purity, morphology, and motility.

Experimental infection. Mice were inoculated orally with 20 µl of viral and/or bacterial stocks, were co-housed in groups of five mice, and were observed daily for clinical signs of infection. Fecal specimens were collected from mice prior to inoculation and at postinoculation days (PID) 7 and 28 for MHV reverse transcriptase-PCR (RT-PCR) analysis and *Helicobacter* PCR. On PID 7 and 28 or when wasting became evident, mice were euthanized by CO_2 inhalation, sera were obtained, and necropsies were performed. All organs were examined for gross lesions, and portions of liver, lung, intestine, brain, and spleen were frozen at –70°C for PCR analysis or were fixed in neutral-buffered 10% formalin and embedded in paraffin. Sections were stained with hematoxylin and eosin (H&E) for histologic examination or were prepared for in situ hybridization (ISH) to detect MHV or *Helicobacter* nucleic acids. Sera were tested for MHV antibodies use of immunofluorescence, as described (30), and by enzyme-linked immunosorbent assay (ELISA), using 75 ng of bacterial expressed MHV-1 N protein/well.

In situ hybridization to detect MHV RNA or *Helicobacter* DNA. In situ hybridization to detect MHV RNA used a gel-purified cDNA of the complete MHV-JHM N gene to gener-

ate a random-primed [^{32}P]-labeled DNA probe. In situ hybridization to detect *Helicobacter* DNA used a [^{32}P]-labeled random-primed PCR product specific for the *Helicobacter* 16S rRNA gene. Hybridization, washing, and visualization conditions were used as described previously (31). The MHV-JHM N gene cDNA also was used to prepare a biotinylated random-primed probe to detect virus by use of immunoperoxidase staining augmented by tyramide amplification (NEN Life Sciences Products, Boston, Mass.) (32)

Molecular diagnostics. The RNeasy kit (Qiagen, Chatsworth, Calif.) was used to extract RNA from liver, brain, lung, spleen, large intestine, or small intestine homogenates or feces. The MHV RT-PCR analysis was performed, using the Superscript One-Step RT-PCR System (Invitrogen, Carlsbad, Calif.). Diagnostic primers used were MN512:GTCATGAGGCTATTCCTACTA and MN1027: ATACACATCTTTGGTGGG . The reaction cycles used for all RT-PCR reactions were as follows: 30 min at 50°C; two min at 94°C; 40 cycles of 15 sec at 94°C, 30 sec at 50°C, and 90 sec at 90°C; and 10 min at 72°C. The RT-PCR products were electrophoresed on a 1% agarose gel, stained with ethidium bromide, and visualized by UV illumination. The specificity of PCR products was confirmed, using restriction enzyme digest analysis.

The primer pairs used for RT-PCR amplification of the MHV-G S gene were MH2146:GACGGATAGCGGTGTTAG and MS1409: GCTTCAGCATATGCAACGTC; MS744: TACTACTTCAGGTGTC and MS2163: CTCACGGGATATGTTG; MS1661:GCGTAGG-TGATCATTG and MS3182:GCACTAATTGCACCAAACCT; and MS2182:GGCTTTGTCGAGGCTTATAA and MS4159:TCTGTC-TTTCCAGGAGAGGC. The primers used for RT-PCR amplification of the 3' end of the MHV-G M gene, intervening sequence, and 5' end of the N gene were MM36:AATCCAAACATTAT-GAGTAG and MN1027:ATACACATCTTTGGTGGG. The primers used for RT-PCR amplification of the 3' end of the MHV-G N gene were MN65:TGGAATCCTCAAGAAGACCAC and RN1476: CGCCCGACATAGGATTCATTCT. Sequencing was performed directly on PCR products at the DNA sequencing facility of the W. M. Keck Foundation Biotechnology Laboratory at the Yale University School of Medicine. The MHV-G S gene PCR products were sequenced, using primers MH2146, MS744, MS1409, MS1661, MS 2163, MS 2812, MS 3182, MS4159 (listed previously), MS445: ATGGCATCCATTTGCC, MS1021: GTACTGT-CTTAGCAGT, MS1026: TCCTCTCAATTGGGAACGCA, and MS1278: GCTCTATTATAGTCTTGCAC. The MHV-G M and N gene PCR products were sequenced, using primers MM36, MN65, MN1027, and RN1476 (listed previously). Sequence comparisons were performed, using tblastx at http://www.ncbi.nlm.nih.gov/BLAST/. Sequences were submitted to Genbank and assigned accession numbers AY102932 (S), AY102933(N), and AY102934(M).

Using the DNeasy Tissue kit (Qiagen, Chatsworth, Calif.), DNA was extracted from liver, brain, lung, spleen, large intestine, or small intestine homogenates or feces. Polymerase chain reaction analysis was performed, using *Taq* polymerase (Roche Molecular Biochemicals, Indianapolis, Ind.) and published primers for *Helicobacter* species 16S rRNA gene (33), *Pneumocystis carinii* 18S mt rRNA gene (34), and *Citrobacter rodentium* attaching and effacing (eae) gene (35). The reaction cycles for all PCR reactions were as follows: 2 min at 94°C; 35 cycles of 30 sec at 94°C, 30 sec at 50°C, and 60 sec at 72°C; and 5 min at 72°C. The PCR products were electrophoresed on 1% agarose gels, stained with ethidium bromide, and visualized by UV illumination. *Helicobacter* PCR products were digested with *Dpn*II and *Hha*I restriction enzymes to differentiate *Helicobacter* species.

Results

Clinical case findings. Within 24 h of importation, 15 C3H- *Ifng* mice developed diarrhea (pasty feces), dehydration (skin turgor assessment), hunched posture, dyspnea, and ruffled pelage. Treatment with moistened rodent chow ameliorated the clinical signs of disease. At postarrival day (PAD) 10, two mice were found dead, and two mice, including one mouse with head tremor, were sent to necropsy for diagnostic assessment. The remaining 11 mice developed a progressive wasting syndrome and were necropsied at PAD 47 (n = 4) and 57 (n = 7).

Mice were tested for the presence of bacterial or viral agents to determine whether the clinical signs of disease were caused by infectious agents. On PAD 10, all mice were culture negative for aerobic bacteria on the liver surface or in the nasopharnyx, cecal contents, and heart blood. On PAD 47, several lung, peritoneal, nasopharyngeal, and cecal specimens were tested and found negative for aerobic bacteria. Mice were screened for antibodies to common murine viruses and were seropositive for MHV only. To ascertain whether mice were actively infected with MHV, RT-PCR analysis for MHV RNA was performed on specimens from animals necropsied on PAD 10 and 47. Mouse hepatitis virus RNA was detected in brain tissue from both mice on PAD 10 and from one of four mice on PAD 47. In addition, MHV RNA was detected in lung, liver, cecum, and colon, confirming active infection in all four mice at PAD 47. Liver, colon, brain, and lung specimens were used to inoculate 17Cl-1, CMT93, J774A.1, L2p176, and NCTC 1469 cells in an attempt to isolate and cultivate the new MHV strain, but cytopathic effects were not observed and inoculated cells were negative for MHV antigens by immunofluorescence and for MHV-RNA by RT-PCR analysis.

Analysis by PCR for *Helicobacter* sp. at PAD 47 detected co-infection of these animals with two *Helicobacter* species, with restriction enzyme digestion patterns consistent with *H. hepaticus* and *H. muridarum* or *H. typhlonicus*. All colons, but no lungs or livers, were *Helicobacter* DNA positive. *Pneumocystis carinii* DNA also was detected in all lung specimens obtained on PAD 47. *Citrobacter rodentium* DNA was not detected in colon or feces at any time point. Microscopic examination of pelt and cecal contents from all mice did not reveal evidence of acariasis or oxyuriasis, respectively.

Gross pathologic findings on PAD 10 included splenomegaly (2/2) and multiple cream-colored foci and exudate on the liver surface (2/2). At PAD 47, lung consolidation was evident in one of four mice. Glistening and granular pleural and peritoneal surfaces, indicators of pleuritis and peritonitis, were present in one of four mice and two of four mice, respectively. Similar pleural (1/7) and peritoneal findings (7/7) were observed on PAD 57. On PAD 47 and 57, mice with peritonitis had extensive adhesions in the peritoneal and pleural cavities.

Histologic examination on PAD 10 revealed mild hepatic lesions that consisted of several areas of acute necrosis with minimal accompanying lymphohistiocytic inflammation. Lesions often were perivascular, adjacent to larger portal veins. Peritoneal, pleural, and pericardial surfaces had variably severe and multifocal inflammation. The inflammatory infiltrate was pre-

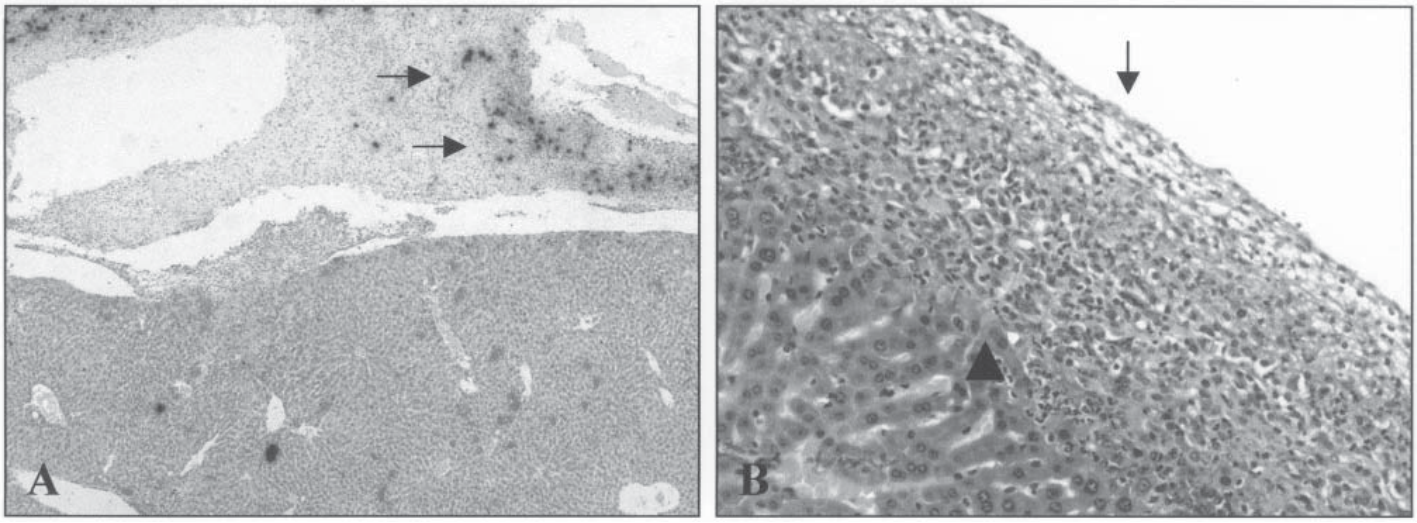

Figure 1. Photomicrographs of liver sections taken from gamma interferon-deficient knockout (IFN-γ KO) mice with clinical infections. (A) Liver from mouse at 10 days after arrival stained with hematoxylin and by in situ hybridization (ISH) for the mouse hepatitis virus N gene. Notice marked fibrinous and predominantly lymphohistiocytic peritonitis, accompanied by abundant viral signal (arrow). Magnification, 100×. (B) Liver from mouse 56 days after arrival stained with hematoxylin and eosin. Peritonitis has assumed chronic-active characteristics—deeper layers adjacent to the liver parenchyma are organizing and contain fibrous tissue and blood vessels (arrowhead), while superficial layers consist of fibrin and neutrophils (arrow). Magnification, 440×.

dominantly lymphohistiocytic; lymphocytes, macrophages, and newly forming blood vessels were present in the deeper layers adjacent to the organ surface, and neutrophils, reactive mesothelial cells, and fibrin exudate were localized superficially (Fig. 1A). On PAD 47 and 57, hepatic lesions had resolved, except for scattered residual inflammation, and enteric lesions were not present. The deeper layers of the peritonitis and pleuritis (Fig. 1B). In the brain, parenchymal lesions were not apparent; however, moderate to severe, predominantly lymphohistiocytic meningitis was present in one mouse. In the kidney of one mouse, there was locally extensive necrosis involving one renal pole that appeared to extend from the surface into the parenchyma, and was accompanied by lymphohistiocytic inflammation.

Use of ISH confirmed that infection included widespread dissemination of MHV to multiple tissues in these mice. At all times, MHV RNA was localized to liver parenchyma surrounding necrotic areas, adjacent to liver vessels, and in serosal inflammation. Mouse hepatitis virus RNA was rarely detected in the enteric lumen or epithelia, or in vessels of the submucosa and muscularis. In the stomach, MHV RNA was localized to the junction of squamous and glandular epithelia in two animals at PAD 47 and 57. At PAD 57, one or more mice had MHV RNA in splenic white pulp, in the left ventricle of the heart, the trachea, pleura, and peribronchia, and in the parenchyma of one lung. To examine cell types infected at PAD 57, a biotinylated probe detected MHV RNA in macrophages in the spleen, kidney, liver; on serosal surfaces; in renal tubular epithelial cells; and in mesothelial cells associated with the serosal inflammation.

In situ hybridization also was performed to detect sites of *Helicobacter* infection because mice were co-infected with *Helicobacter* sp. On PAD 10, *Helicobacter* DNA was detected in the intestinal lumen, principally in intestinal contents, and less commonly on the surface of superficial enterocytes. On PAD 57, *Helicobacter* DNA was detected principally in intestinal contents and sporadically in the liver parenchyma; it was not detected in the inflammatory lesions associated with liver or serosal surfaces.

Table 1. Amino acid comparisons among mouse hepatitis virus strain G (MHV-G) and other rodent coronaviruses

Coronavirus	S protein[a]	M protein[b]	N protein[c]
MHV-Y	**98.3**	**98.7**	**97.5**
MHV-TY	**96.2**	**97.3**	**96.1**
MHV-DVIM	**95.0**	**97.3**	**95.0**
MHV-2	92.7	**97.3**	92.2
RCV-SDA	92.1	**95.6**	91.9
MHV-RI	83.2	94.6	**97.2**
MHV-4	83.1	**96.4**	92.8
MHV-A59	80.6	**98.2**	**96.6**

Identity percentages were determined, using tblastx, and identities ≥ 95% are indicated in boldface type.
[a]Comparison of 1,361 amino acids of S.
[b]Comparison of 223 amino acids of M.
[c]Comparison of 359 amino acids of N.

Molecular characterization of MHV-G. To determine whether the MHV strain infecting these mice was a new or previously identified strain of MHV, sequence analysis was performed. The RT- PCR products from the following regions of MHV-G—the entire 4,086 bp of the S gene, 669 bp of the M gene (all but the 13 nucleotides at the 5' end of the M gene), and 1,077 bp of the N gene (comparable to nucleotides 244 to 1320 of the MHV-Y N gene)—were sequenced. The predicted S, M, and N protein sequences for MHV-G were compared with those of other MHV strains; MHV-G was determined to be a new MHV strain, and its S, M, and N proteins had the highest degree of identity with those of MHV-Y, a naturally occurring enterotropic MHV strain (Table 1).

Experimental reproduction of peritonitis and pleuritis in mice. An experiment was performed to reproduce the clinical disease and initiate analysis of the infectious agent(s) causing the unusual peritonitis and pleuritis. Cecal homogenate from a clinically ill mouse at PAD 47, containing MHV-G and *Helicobacter* species, but not *Pneumocystis carinii*, was used to inoculate 10 IFN-γ KO mice. Host background was changed from C3H to BALB/c because C3H IFN-γ KO mice were not

Table 2. Summary of the experimentally induced infections

	BALB/c		IFN-γ	
Day after co-inoculation	14	28	14	28
MHV Serology	5/5*	5/5	3/5	5/5
Fecal MHV RT-PCR	10/10	3/5	10/10	1/5
Fecal *Helicobacter* PCR	0/10	2/5	2/10	5/5
Hepatitis	2/5	0/5	2/5	0/5
Peritonitis	0/5	0/5	4/5	5/5
Pleuritis	0/5	0/5	2/5	5/5
Encephalitis	0/5	0/5	0/5	0/5

*Number of positive mice/ total number of mice.
MHV = mouse hepatitis virus; PCR = polymerase chain reaction (analysis); RT = reverse transcriptase.

commercially available. Ten BALB/c mice were inoculated to determine whether peritonitis and pleuritis develops in immunocompetent mice. In addition, five nude mice were inoculated to amplify the viral stock and determine whether the absence of an adaptive immune response contributes to the development of peritonitis, pleuritis, and adhesions.

All inoculated IFN-γ KO mice had ruffled pelage and loose feces at postinoculation day (PID) 14. All 10 mice were shedding MHV in the feces, two of 10 were shedding *H. hepaticus*, and three of five were MHV seropositive (Table 2). Pale liver, with or without white foci, was observed in four of five mice at necropsy. Microscopically, mice had necrosuppurative hepatitis, multifocal suppurative peritonitis, and focal suppurative pleuritis (Table 2). Also, four of five mice had gut-associated lymphoid tissue (GALT) hyperplasia. By PID 28, all IFN-γ KO mice were seropositive for MHV. One of five mice was shedding MHV, and all were shedding *H. hepaticus*. Pleural and peritoneal adhesions were evident at necropsy in two of five mice. Microscopically, all mice had multifocal subacute suppurative peritonitis and pleuritis (Table 2), two mice had GALT hyperplasia, and one mouse had mild meningitis. The peritoneal and pleural lesions observed in the experimentally infected IFN-γ KO mice were similar to those observed in the naturally infected C3H-*Ifng* mice.

Clinical signs of disease were not seen in inoculated immunocompetent BALB/c mice at PID 14 or 28. At PID 14, all BALB/c mice were MHV seropositive and shedding MHV-G, but not *H. hepaticus* in the feces (Table 2). Microscopically, two of five mice had mild focal subacute suppurative hepatitis, but there was no evidence of peritonitis or pleuritis. At PID 28, three of five BALB/c mice were shedding MHV-G and two of five were shedding *H. hepaticus* in the feces. Microscopically, there was no evidence of hepatitis, peritonitis, or pleuritis. Thus, MHV-G and *H. hepaticus* caused only mild acute disease in BALB/c mice.

Clinical signs of infection were not evident in nude mice at PID 14, but all mice were shedding MHV-G and *H. hepaticus* in the feces. Between PID 18 and 22, nude mice developed hunched posture, lethargy, and dehydration, and three of five mice died between PID 21 and 22. On PID 22, the remaining two mice continued to shed MHV-G and *H. hepaticus* in the feces, and small and large intestines, lung, liver, and brain were RT-PCR positive for MHV. Microscopically, both mice had moderate to severe multifocal necrotizing hepatitis, splenic necrosis, and necrotizing multifocal encephalitis. Unlike IFN- γ KO mice, lesions in all organs of nude mice had syncytia, and there was no evidence of peritonitis, pleuritis, or adhesions (data not shown). The disease in these mice was similar to the "chronic wasting syndrome" described in a clinical study by Sebesteny in which nude mice were infected with MHV (36).

Table 3. Experimentally induced infections in interferon gamma-deficient knockout (IFN-γ KO) mice with MHV-G alone or along with *H. hepaticus*

	MHV		*Helicobacter* and MHV[a]		*Helicobacter* then MHV[b]	
Day after MHV inoculation	7	28	7	28	7	28
Mortality	5/16*	0/6	2/15	0/8	0/15	0/10
Hepatitis	5/5	1/6	2/5	4/8	4/5	5/10
Peritonitis	5/5	6/6	0/5	7/8	3/5	10/10
Pleuritis	0/5	5/6	0/5	4/7	0/5	6/10
Adhesions	0/5	6/6	0/5	7/8	0/5	9/10
Meningitis	2/5	4/6	1/5	8/8	1/5	6/10
Enteritis	5/5	0/6	3/5	0/8	5/5	0/10
Cecal MHV RT-PCR	5/5	5/6	3/5	3/8	5/5	0/10
Liver MHV RT-PCR	5/5	0/6	3/5	3/8	5/5	1/10
Cecal *Helicobacter* PCR	0/5	0/6	2/5	8/8	5/5	9/10

*Number of positive mice/ total mice.
[a]*Helicobacter* and MHV simultaneous inoculation.
[b]*Helicobacter* inoculation 28 days prior to MHV inoculation.
See Table 2 for key.

Experimentally induced infections to determine individual roles of MHV-G and *H. hepaticus* in the formation of pleural and peritoneal lesions. The previous experiment confirmed that the cecal inoculum from the clinical infections contained the infectious agent(s) necessary to reproduce the disease in IFN-γ KO mice, but the roles of MHV-G and *Helicobacter* species in the clinical syndrome still needed to be delineated. Therefore, infection of IFN-γ KO mice with MHV-G and *Helicobacter* sp. separately or together was examined in greater detail. Liver homogenates obtained from infected nude mice at PID 22 were analyzed by PCR analysis and were found to contain MHV RNA, but not *Helicobacter* DNA. This liver homogenate and/or cultured *H. hepaticus* were used as inocula to compare pathogenesis and infection in four groups of IFN-γ KO mice inoculated with: MHV-G alone, *H. hepaticus* alone, MHV-G and *H. hepaticus* simultaneously, and *H. hepaticus* 28 days before inoculation with MHV-G.

Clinical disease, including ruffled pelage, was evident in all IFN-γ KO mice inoculated with MHV-G, with or without *H. hepaticus*, on PID 6 to 8. Mortality was evident between PID 7 and 12, and was highest in mice inoculated with MHV-G alone (Table 3). Clinical disease or mortality was not observed in mice inoculated with *H. hepaticus* only (data not shown). All mice inoculated with MHV were seronegative at PID 7, but all were seropositive at PID 28.

MHV-G Infection. On PID 7 and 28, microscopic findings from IFN-γ KO mice inoculated with MHV-G alone were similar to those seen in the clinical cases (Table 3). On PID 7, pathologic changes included multifocal hepatic necrosis accompanied by predominantly suppurative inflammation. Foci of necrosis were most commonly located adjacent to portal veins (Fig. 2A). Although qualitatively similar, the severity of lesions varied among mice. In small intestine, cecum, and colon, acute necrotizing and inflammatory lesions were present. These were characterized by epithelial necrosis at all levels of the intestinal glands and crypts (Fig. 2B). Necrotic debris, accompanied by an inflammatory infiltrate composed of macrophages, lymphocytes, and neutrophils, was present in the lamina propria and submucosa (Fig. 2B). In locations where inflammation extended through the muscularis mucosae to reach the serosa, acute peritonitis involved the serosal surface of the intestine. Additionally, GALT was greatly expanded by lymphoid hyperplasia and mixed histiocytic/neutrophilic inflammation accompanied by necrosis (Fig. 2C). In some mice, mild lymphohistiocytic meningitis with rare parenchymal necrosis was present in the brain and splenic necrosis was observed in the white pulp.

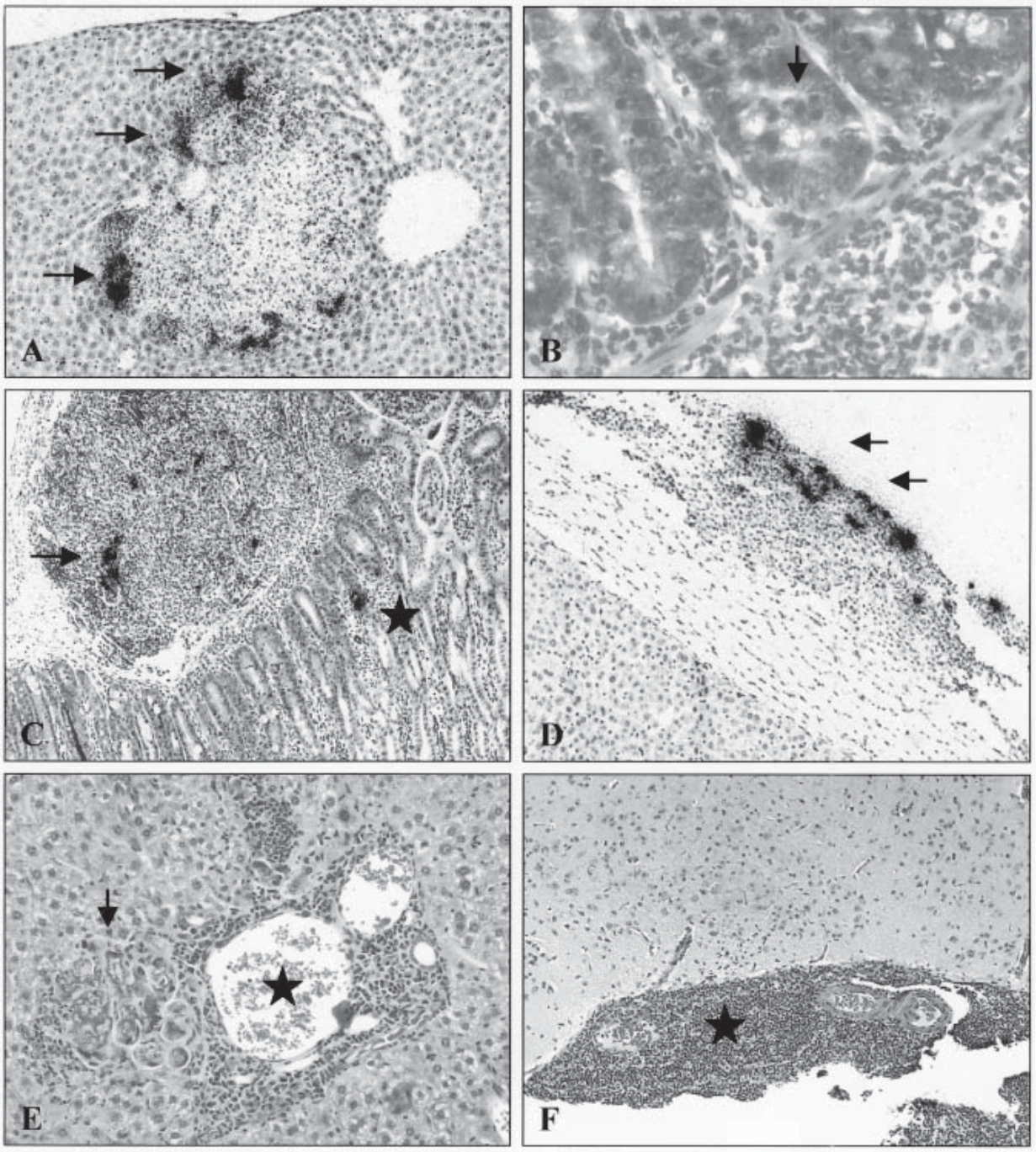

Figure 2. Photomicrographs of sections of tissues taken from IFN-γ KO mice with experimentally induced infections. (A) Liver from mouse infected with mouse hepatitis virus alone at postinoculation day 7, stained with hematoxylin and by in situ hybridization for the mouse hepatitis virus N gene. Necrotic foci are typically located adjacent to portal veins. Necrosis is accompanied by minimal inflammation, and mouse hepatitis virus signal is present at necrotic borders (arrows). (B) Small intestine from mouse infected with mouse hepatitis virus alone at postinoculation day 7, and stained with hematoxylin and eosin . Single-cell enterocyte necrosis is present at all levels of the glands (arrow), and is accompanied by infiltration of predominantly neutrophils into the lamina propria and submucosa (lower right hand corner). (C) Small intestine from mouse infected with mouse hepatitis virus alone at postinoculation day 7, and stained with hematoxylin and by in situ hybridization for the mouse hepatitis virus N gene. Notice marked expansion of gut-associated lymphoid tissue by a mixed neutrophilic and lymphohistiocytic population. This is accompanied by viral signal (arrow). Virus is also apparent in enterocytes (asterisk). (D) Liver from mouse infected with mouse hepatitis virus alone at postinoculation day 28, and stained with hematoxylin and by in situ hybridization for the mouse hepatitis virus N gene. Hepatic lesions have resolved, but organizing peritonitis and pleuritis have resulted in adhesions between diaphragm and liver. Viral signal is present in inflammatory infiltrates (arrows). (E) Liver from mouse infected with mouse hepatitis virus and *Helicobacter hepaticus* simultaneously at postinoculation 28, and stained with hematoxylin and eosin. Notice residual inflammation characterized by plasma cells, lymphocytes, and macrophages, typically around blood vessels (asterisk). Large macrophages engorged with intracytoplasmic debris and mineral remain at sites of necrosis (arrow). (F) Brain from mouse infected with mouse hepatitis virus and *H. hepaticus* simultaneously at postinoculation 28, and stained with hematoxylin and eosin. Notice marked suppurative meningitis (asterisk). Magnification: A, C, D, E, and F, 190×; B, 380×.

In situ hybridization and RT-PCR analysis were used to correlate viral infection with necrotic and inflammatory lesions in tissues. At PID 7, hepatic lesions contained many MHV RNA-positive cells, particularly at the periphery of necrotic foci (Fig. 2A), and all liver specimens were positive for MHV RNA by RT-PCR analysis. In the small intestine, cecum, and colon, MHV RNA was detected on serosal surfaces and in epithelial cells, lamina propria, muscularis mucosae, and GALT (Fig. 2C), and all cecal specimens were MHV RNA positive by use of RT-PCR analysis. A biotinylated probe detected MHV RNA in intestinal epithelial cells, macrophages, and smooth muscle cells of the muscularis mucosae. In the spleen, MHV RNA was detected in red and white pulp of all mice. In the brain parenchyma, neuronal and glial cells contained MHV RNA.

By PID 28, parenchymal lesions in the liver had resolved and ISH detected low numbers of cells contained MHV RNA. Enteric lesions had nearly resolved, there was no detectable epithelial necrosis, and inflammation was minimal. Mouse hepatitis virus RNA was detected by ISH in the gut lumen, and occasionally, on the luminal surface of epithelial cells, and RT-PCR analysis detected MHV-RNA in five of six cecal specimens. Mild to moderate chronic active organizing peritonitis and pleuritis resulted in adhesions among the viscera (Fig. 2D). Mouse hepatitis virus RNA was consistently present in inflammatory infiltrates, particularly at serosal surfaces where inflammation was most acute (Fig. 2D). In the spleen, marked white pulp hyperplasia was present, but MHV RNA was not detected. In the brain of several mice, MHV RNA and mild to moderate meningitis persisted. Scattered pockets of infection were infrequently observed at other sites. This group remained *Helicobacter* free as *Helicobacter* DNA was not detected in the cecum or liver of these mice.

***Helicobacter hepaticus* infection.** In contrast to results obtained after MHV infection, IFN-γ KO mice inoculated with *H. hepaticus* alone had minimal pathologic changes (data not shown). At PID 56, relevant histologic lesions, including peritonitis or hepatitis, were not present in any examined tissue. The absence of hepatitis was not unexpected as *H. hepaticus*-induced hepatic lesions are generally not evident until postinoculation months 3 to 6. Use of ISH detected *Helicobacter* DNA in hepatic parenchyma without inflammation, in gut contents, and on the surface of enterocytes. Cecal, but not liver specimens were PCR positive for *Helicobacter* DNA. The negative *Helicobacter* PCR results, compared with the positive *Helicobacter* ISH results for liver, may have been due to specimen location in the liver or to PCR inhibitors. Thus, chronic-active peritonitis and/or pleuritis and formation of adhesions were specific to MHV infection.

Inoculation of MHV-G and *H. hepaticus* on the same day. At seven days after simultaneous inoculation with MHV-G and *H. hepaticus*, lesions were less severe and less frequently observed in co-infected mice and were principally present in the liver and gastrointestinal tract (Table 3). Two mice had hepatitis with lymphohistiocytic infiltrates surrounding areas of necrosis; in one case, lesions were mild to moderate, and in the other, lesions were severe with syncytia. Analysis by RT-PCR , however, demonstrated that three of five liver specimens contained MHV RNA. Enteric lesions qualitatively resembled those in mice infected with MHV alone, but were less severe and present in fewer mice.

Lesions were characterized by scattered single-enterocyte necrosis accompanied by modest accumulation of mixed inflammatory cells in the lamina propria. Inflammatory lesions were most prominent in the small intestine and were characterized by edema of the lamina propria, dilatation of lacteals, and marked expansion of GALT by histiocytes, neutrophils, and necrotic debris. Enteric necrosis was most evident in the cecum; however, inflammation was less severe in this location than in the small intestine. Syncytia were seen only in the cecum, and three of five specimens were MHV RNA positive by RT-PCR analysis. Mild to moderate meningitis was present in a few animals, and the spleen was minimally affected in this group.

By PID 28, the incidence of hepatitis was higher in co-infected mice than in mice infected with MHV-G alone (Table 3). Hepatic lesions were mild to moderate, and consisted principally of multifocal hepatitis with histiolymphocytic infiltrate and scattered foci of syncytial cells (Fig. 2E). Mouse hepatitis virus RNA was detected by RT-PCR analysis in three of eight liver specimens, but *Helicobacter* DNA was not detected by PCR analysis. Intestinal lesions had resolved entirely, although three of eight cecal specimens were MHV RNA positive by RT-PCR analysis, and all cecal specimens were *Helicobacter* DNA positive by PCR analysis. There was marked peritonitis and pleuritis, with adhesions among abdominal and thoracic organs, and lesions varied from organized fibrous tissue with minimal lymphohistiocytic infiltrate to a chronic-active process, with mixed inflammatory cells. In contrast to mice inoculated with MHV-G alone, most had mild to moderate meningitis, and two had severe, suppurative meningitis (Fig. 2F).

Inoculation with *H. hepaticus* 28 days prior to inoculation with MHV-G. The IFN-γ KO mice were inoculated with *H. hepaticus* followed by inoculation with MHV 28 days later to examine the impact of established *Helicobacter* infection on MHV-G infection. Lesions at post MHV inoculation day (PMID) 7 (post *Helicobacter hepaticus* inoculation day (PHID) 35) resembled those associated with the acute stages of MHV infection alone (Table 3). Liver lesions were intermediate in severity, compared with those of the other groups, being less severe than those in mice of the MHV-G alone group and being more severe than those in simultaneously infected mice. Hepatitis was characterized by acute multifocal necrosis with suppurative inflammation. Enteric lesions were characterized by scattered enterocyte necrosis and syncytia, particularly in the cecum. This was accompanied by variable mixed inflammation of the submucosa and lamina propria, with scattered necrosis. Inflammation tended to be more severe in the small intestine, with marked expansion of GALT and occasional herniation of glands into the GALT. Lesions were not detected in most of the brains, although one mouse had focal lymphohistiocytic ventriculitis. In the spleen, there was marked white pulp hyperplasia in all mice. Using ISH, MHV RNA was localized to areas of hepatic necrosis in a few mice, and all mice were MHV RNA positive by RT-PCR analysis. In the GI tract, ISH localized MHV RNA to enterocytes, submucosa, muscularis mucosae, serosa, and GALT, and all cecal specimens were MHV RNA positive by RT-PCR analysis. Use of ISH detected MHV RNA in the meninges and brain parenchyma of several mice; *Helicobacter* DNA was detected by ISH predominantly in gut contents and rarely on the surface of enterocytes throughout the GI tract, and all cecal specimens were DNA positive by PCR analysis.

At PMID 28 (PHID 56), mice had mild to moderate multifocal hepatitis with lymphohistiocytic infiltrate (Table 3) although only

one liver specimen was MHV positive by RT-PCR analysis. Enteric lesions had resolved except for residual lymphohistiocytic infiltrate of the lamina propria. Chronic-active peritonitis and pleuritis with adhesions were present in most mice. Splenic hyperplasia was present in all mice. In the brain, mild to moderate meningitis was present in half of the mice. Use of ISH detected MHV RNA in hepatocytes, mucosa of cecum, and serosal inflammatory infiltrates and vasculature. In a few mice, MHV RNA also was detected in the parenchyma of the lung, pyloric epithelium, parenchyma and meninges of the brain, and renal tubular epithelial cells. Using ISH, *Helicobacter* DNA was localized to gut contents and the surface of intestinal and cecal mucosa.

Discussion

Results of our experiments confirmed that the initial clinical disease was due to infection of IFN-γ KO mice with an enterotropic strain of MHV. Experimental inoculation of cecal homogenate, containing MHV and *H. hepaticus*, from a clinically infected mouse into IFN-γ KO mice resulted in development of chronic-active peritonitis and/or pleuritis with adhesions, necrosuppurative hepatitis, and GALT hyperplasia. Immunocompetent BALB/c mice did not develop a similar disease after infection, indicating a role for IFN-γ deficiency in the disease process and the necessity for an intact immune system in viral clearance. In the case of the clinical infection, time of infection with either MHV or *H. hepaticus* is unknown. Imported mice presumably had established *Helicobacter* infection prior to virus infection, as most mouse colonies were enzootically infected at that time. However, the hepatitis with inflammation observed in the clinical cases at PAD 10 correlates with the disease in the IFN-γ KO mice 14 days after inoculation with the cecal homogenate. Given these similarities, mice probably were exposed to MHV a short time before or during shipment. By use of sequence analysis, we confirmed that the cecal homogenate contained a previously uncharacterized strain of MHV that was most closely related to MHV-Y, an enterotropic strain also isolated from a clinical outbreak. Infection of BALB/c mice confirmed the enterotropic phenotype of MHV-G because it was restricted to the GI tract of immunocompetent mice.

Clinically infected mice were positive for MHV RNA and *H. hepaticus* DNA; therefore, experiments were designed to determine which agent(s) was responsible for development of peritonitis and pleuritis. Mice experimentally infected with *H. hepaticus* alone did not manifest clinical signs of infection or microscopic lesions at PID 56. As was seen in the clinical cases, most MHV-infected mice at PID 7 had hepatic necrosis with inflammation and without syncytia, GALT hyperplasia, enteritis, and cecal necrosis with syncytia formation. All MHV-infected groups at PMID 28 had chronic-active, organizing peritonitis and pleuritis with adhesions. Mouse hepatitis virus RNA was present in the peritonitis and pleuritis lesions and adhesions, indicating that the serosal surfaces are sites of persistent virus infection. As a result of this study, we can conclude that MHV infection of IFN-γ KO mice in the presence or absence of *H. hepaticus* results in peritonitis and pleuritis progressing to the formation of abdominal and thoracic adhesions.

Although MHV and *H. hepaticus* are enterotropic, previous reports of MHV infection in IFN-γ KO mice did not address the possibility of *Helicobacter* co-infection or its potential for modulating MHV pathogenesis. One example of virus-*Helicobacter* interference was reported by Jiang and co-workers (37). They found that infection with a replication-deficient adenovirus decreased numbers of *H. felis* in the stomach of C57BL/6 but not IFN-γ- or interleukin 12 -deficient mice, and concluded that Th1 responses associated with a systemic viral infection can influence established *Helicobacter* infection.

Our results indicated that co-infection of IFN-γ KO mice with MHV-G and *H. hepaticus* modified the pathogenesis of MHV infection, and time of *H. hepaticus* infection further affected the results. Inoculation with *H. hepaticus* and MHV reduced mortality, compared with that associated with inoculation with MHV-G alone. Acute disease in groups infected with both agents was qualitatively similar to that associated with MHV alone, but numbers of mice with lesions and the severity of lesions were lower in both co-infected groups at PMID 7. Therefore, infection with *H. hepaticus* and the resultant immune response to *H. hepaticus* appears to reduce the severity of lesions during the acute phase of the disease.

In contrast, the later phase of the disease appears more severe in mice infected with both agents. At PMID 28, all mice simultaneously infected with MHV-G and *H. hepaticus* had moderate to severe meningitis, compared with lower incidences of mild meningitis in the two other groups. The increased incidence of meningitis could be caused by higher levels of viremia resulting from the impact of co-infection on gut epithelia and the host immune response. Hepatitis persisted in half of the mice from both co-infected groups, whereas one mouse infected with MHV-G alone had hepatic lesions. Presence of MHV RNA and syncytia in the liver of simultaneously co-infected mice suggests ongoing viral infection in this group. In contrast, there were no syncytia, and only one liver from the group infected with *H. hepaticus* before MHV contained MHV RNA, suggesting that MHV-G had been cleared from lesions. Less severe disease at PMID 7 and more severe disease at PMID 28 in MHV-G and *H. hepaticus* co-infected mice may result from altered replication kinetics due to interference between two intestinal pathogens that co-localize to a similar intestinal region during infection. In addition, increased immune cell infiltration or cytokine levels during dual infection may affect the kinetics of MHV replication. Future experiments using intermediate time points will be necessary to define the kinetics of disease progression in the different groups.

Although granulomatous peritonitis and pleuritis are not typical MHV lesions in immunocompetent or immunocompromised mice, they also have been reported after natural or experimentally (intraperitoneal route) induced MHV infection in C57BL/6 IFN-γ KO mice (14, 15). In those reports in contrast to our report, peritonitis also included ascites generation and formation of pseudomembraneous "cocoons", and mice infrequently developed meningitis. Although our results were similar after oral inoculation of MHV-G into C3H IFN-γ KO and BALB/c IFN-γ KO mice, Kyuwa and co-workers (15, 16) found that MHV-JHM pathogenesis in IFN-γ KO mice can be influenced by host genotype. After intraperitoneal inoculation of MHV, C57BL/6 IFN-γ KO mice develop granulomatous peritonitis and pleuritis while BALB/c IFN-γ KO mice develop acute hepatic failure with 100% mortality by one week. An additional group described intraperitoneal inoculation of MHV-A59 in 129 IFN-γ receptor KO mice, and the outcome was early, severe hepatitis and mortality in the absence of peritoneal or pleural lesions (17, 38). Although those

results differ from ours, use of different strains of coronavirus, mouse genotype, and route of inoculation could explain these disparities.

The role of IFN-γ in resolution of enterotropic MHV infection is unknown. Gamma interferon is synthesized by natural killer cells and T lymphocytes following their activation by IL-12 or IL-18. It activates macrophages, natural killer cells, and endothelial cells; increases class-I and class-II MHC expression; and promotes B- and T-lymphocyte differentiation. The resultant Th1 cellular response and macrophage-rich inflammatory reaction contribute to protection against viral and intracellular bacterial infections (9). Although IFN-γ KO mice would not be expected to mount an adequate Th1 response, this was not the case after experimentally induced influenza. An effective Th1 response was mounted that included virus-specific $CD4^+$ and $CD8^+$ T lymphocytes that were cytolytic in vitro and protective in vivo (39). In the case of polytropic MHV infection of C57BL/6 IFN-γ KO mice, neither cytotoxic T lymphocyte responses nor antiviral antibody were diminished in the absence of IFN-γ (40). As described in the results for MHV-G infected mice, resolution of hepatitis and enteritis indicates a functional cellular response to the virus. However, development of peritonitis and pleuritis with adhesions may result from impaired function of and continued viral infection in macrophages. Mouse hepatitis virus replicates in monocytes and macrophages, and cytolytic infection of these cells in IFN-γ KO mice may result in increased recruitment of granulocytes and macrophages to the sites of peritonitis. This could result in increased targets for continued virus replication, unchecked expansion of lesions, and establishment of adhesions within the peritoneal and pleural cavities. It is important to note that induction of peritonitis requires the combination of IFN-γ deficiency and MHV infection, as other viral or bacterial infections in IFN-γ-deficient mice and MHV infection of other immunodeficient or immunocompetent mouse strains do not result in peritonitis or pleuritis. From these studies, it is unclear whether infection of IFN-γ KO mice with other enterotropic MHV strains would result in pleuritis and peritonitis, but given that two other MHV strains have been reported to cause peritonitis in IFN-γ KO mice (14, 15), it is likely that natural infection of IFN-γ KO mice with other enterotropic MHV strains would also result in peritonitis and pleuritis.

This study confirmed that enterotropic MHV infection of IFN-γ KO mice resulted in peritonitis and pleuritis with adhesions. Additionally, it indicated that infection of these mice with *H. hepaticus* altered the pathogenesis of MHV. Since coronaviruses and *Helicobacter* species are a significant cause of gastrointestinal tract disease in humans and animals, understanding the mechanism of viral modulation in bacterial co-infection will help elucidate factors that impact gastrointestinal tract disease. In future experiments, we will advance this model of *H. hepaticus* and MHV co-infection in immunocompetent and immunocompromised mice to determine the mechanisms and impact of co-infection on induction and exacerbation of gastrointestinal tract disease, including inflammatory bowel disease.

Acknowledgments

We thank Nirah Shomer for providing *Helicobacter hepaticus* cultures. We also thank Frank Paturzo and Beatriz Vivas-Gonzalez for technical assistance.

References

1. **Barthold, S. W., A. L. Smith, P. F. Lord, P. N. Bhatt, R. O. Jacoby, and A. J. Main.** 1982. Epizootic coronaviral typhlocolitis in suckling mice. Lab. Anim. Sci. **32:**376-383.
2. **Barthold, S. W., D. S. Beck, and A. L. Smith.** 1993. Enterotropic coronavirus (mouse hepatitis virus) in mice: influence of host age and strain on infection and disease. Lab. Anim. Sci. **43:**276-284.
3. **Compton, S. R.** 2002. Unpublished data.
4. **Barthold, S. W., A. L. Smith, and M. L. Povar.** 1985. Enterotropic mouse hepatitis virus infection in nude mice. Lab. Anim. Sci. **35:**613-618.
5. **Yanagisawa, T., K. Nakanaga, S. Kyuwa, and K. Fujiwara.** 1985. Ascitic disease in nude mice infected with mouse hepatitis virus. Jpn. J. Vet. Sci. **47:**171-174.
6. **Compton, S. R., S. W. Barthold, and A. L. Smith.** 1993. The cellular and molecular pathogenesis of coronaviruses. Lab. Anim. Sci. **43:**15-28.
7. **Jacoby, R. O. and J. R. Lindsey.** 1997. Health care for research animals is essential and affordable. FASEB J. **11:**609-614.
8. **Homberger, F. R.** 1998. Prevalence of enterotropic and polytropic mouse hepatitis virus in enzootically infected mouse colonies. Lab. Anim. Sci. **48:**50-54.
9. **Shtrichman, R., and C. E. Samuel.** 2001. The role of gamma interferon in antimicrobial immunity. Curr. Opin. Microbiol. **4:**251-259.
10. **Moore, T., M. Perry, A. Getsoian, M. Newstead, and T. Standiford.** 2002. Divergent role of gamma interferon in a murine model of pulmonary versus systemic *Klebsiella pneumoniae* infection. Infect. Immun. **70:**6310-6318.
11. **Shinozawa, Y., T. Matsumoto, K. Uchida, S. Tsujimoto, Y. Iwakura, and K. Yamaguchi.** 2002. Role of interferon-gamma in inflammatory response in murine respiratory infection with *Legionella pneumophila.* J. Med. Microbiol. **51:**225-230.
12. **Geiger, K. D., T. C. Nash, S. Sawyer, T. Krahl, G. Patstone, J. C. Reed, S. Krajewski, D. Dalton, M. J. Buchmeier, and N. Sarvetnick.** 1997. Interferon-gamma protects against herpes simplex virus type 1-mediated neuronal death. Virology **238:**189-197.
13. **Bartholdy, C., J. P. Christensen, D. Wodarz, and A. R. Thomsen.** 2000. Persistent virus infection despite chronic cytotoxic T-lymphocyte activation in gamma interferon-deficient mice infected with lymphocytic choriomeningitis virus. J. Virol. **74:**10304-10311.
14. **France, M. P., A. L. Smith, R. Stevenson, and S. W. Barthold.** 1999. Granulomatous peritonitis and pleuritis in interferon-gamma gene knockout mice naturally infected with mouse hepatitis virus. Aust. Vet. J. **77:**600-604.
15. **Kyuwa, S., Y. Tagawa, S. Shibata, K. Doi, K. Machii, and Y. Iwakura.** 1998. Murine coronavirus-induced subacute fatal peritonitis in C57BL/6 mice deficient in gamma interferon. J. Virol. **72:**9286-9290.
16. **Kyuwa, S., S. Shibata, Y. Tagawa, Y. Iwakura, K. Machii, and T. Urano.** 2002. Acute hepatic failure in IFN-gamma-deficient BALB/c mice after murine coronavirus infection. Virus Res. **83:**169-177.
17. **Schijns, V. E., C. M. Wierda, M. van Hoeij, and M. C. Horzinek.** 1996. Exacerbated viral hepatitis in IFN-gamma receptor-deficient mice is not suppressed by IL-12. J. Immunol. **157:**815-821.
18. **Fox, J. G., L. Yan, B. Shames, J. Campbell, J. C. Murphy, and X. Li.** 1996. Persistent hepatitis and enterocolitis in germfree mice infected with *Helicobacter hepaticus*. Infect. Immun. **64:**3673-3681.
19. **Ward, J. M., M. R. Anver, D. C. Haines, J. M. Melhorn, P. Gorelick, L. Yan, and J. G. Fox.** 1996. Inflammatory large bowel disease in immunodeficient mice naturally infected with *Helicobacter hepaticus*. Lab. Anim. Sci. **46:**15-20.
20. **Cahill, R. J., C. J. Foltz, J. G. Fox, C. A. Dangler, F. Powrie, and D. B. Schauer.** 1997. Inflammatory bowel disease: an immunity-mediated condition triggered by bacterial infection with *Helicobacter hepaticus*. Infect. Immun. **65:**3126-3131.

21. **Foltz, C. J., J. G. Fox, R. Cahill, J. C. Murphy, L. Yan, B. Shames, and D. B. Schauer.** 1998. Spontaneous inflammatory bowel disease in multiple mutant mouse lines: association with colonization by *Helicobacter hepaticus*. Helicobacter **3:**69-78.
22. **Maggio-Price, L., D. Shows, K. Waggie, A. Burich, W. Zeng, S. Escobar, P. Morrissey, and J. L. Viney.** 2002. *Helicobacter bilis* infection accelerates and *H. hepaticus* infection delays the development of colitis in multiple drug resistance-deficient (mdr1a-/-) mice. Am. J. Pathol. **160:**739-751.
23. **Ihrig, M., M. D. Schrenzel, and J. G. Fox.** 1999. Differential susceptibility to hepatic inflammation and proliferation in AXB recombinant inbred mice chronically infected with *Helicobacter hepaticus*. Am. J. Pathol. **155:**571-582.
24. **Whary, M. T., J. Cline, A. King, Z. Ge, Z. Shen, B. Sheppard, and J. G. Fox.** 2001. Long-term colonization levels of *Helicobacter hepaticus* in the cecum of hepatitis-prone A/JCr mice are significantly lower than those in hepatitis-resistant C57BL/6 mice. Comp. Med. **51:**413-417.
25. **Whary, M. T., T. J. Morgan, C. A. Dangler, K. J. Gaudes, N. S. Taylor, and J. G. Fox.** 1998. Chronic active hepatitis induced by *Helicobacter hepaticus* in the A/JCr mouse is associated with a Th1 cell-mediated immune response. Infect. Immun. **66:**3142-3148.
26. **Kullberg, M. C., J. M. Ward, P. L. Gorelick, P. Caspar, S. Hieny, A. Cheever, D. Jankovic, and A. Sher.** 1998. *Helicobacter hepaticus* triggers colitis in specific-pathogen-free interleukin-10 (IL-10)-deficient mice through an IL-12- and gamma interferon-dependent mechanism. Infect. Immun. **66:**5157-5166.
27. **Kullberg, M. C., A. G. Rothfuchs, D. Jankovic, P. Caspar, T. A. Wynn, P. L. Gorelick, A. W. Cheever, and A. Sher.** 2001. *Helicobacter hepaticus*-induced colitis in interleukin-10-deficient mice: cytokine requirements for the induction and maintenance of intestinal inflammation. Infect. Immun. **69:**4232-4241.
28. **Kullberg, M. C., D. Jankovic, P. L. Gorelick, P. Caspar, J. J. Letterio, A. W. Cheever, and A. Sher.** 2002. Bacteria-triggered CD4(+) T regulatory cells suppress *Helicobacter hepaticus*-induced colitis. J. Exp. Med. **196:**505-515.
29. **Sawai, N., M. Kita, T. Kodama, T. Tanahashi, Y. Yamaoka, Y. Tagawa, Y. Iwakura, and J. Imanishi.** 1999. Role of gamma interferon in *Helicobacter pylori*-induced gastric inflammatory responses in a mouse model. Infect. Immun. **67:**279-285.
30. **Smith, A. L.** 1983. An immunofluorescence test for detection of serum antibody to rodent coronaviruses. Lab. Anim. Sci. **33:**157-160.
31. **Ball-Goodrich, L. J., S. E. Leland, E. A. Johnson, F. X. Paturzo, and R. O. Jacoby.** 1998. Rat parvovirus type 1: the prototype for a new rodent parvovirus serogroup. J. Virol. **72:**3289-3299.
32. **Jacoby, R. O., E. A. Johnson, F. X. Paturzo, and L. Ball-Goodrich.** 2000. Persistent rat virus infection in smooth muscle of euthymic and athymic rats. J. Virol. **74:**11841-11848.
33. **Riley, L. K., C. L. Franklin, R. R. Hook, Jr., and C. Besch-Williford.** 1996. Identification of murine helicobacters by PCR and restriction enzyme analyses. J. Clin. Microbiol. **34:**942-946.
34. **Wakefield, A., F. Pixley, S. Banerji, S. Sinclair, R. Miller, E. Moxon, and J. Hopkin.** 1990. Detection of *Pneumocystis carinii* with DNA amplification. Lancet **336:**451-453.
35. **Schauer, D. and S. Falkow.** 1993. Attaching and effacing locus of *Citrobacter freundii* biotype that causes transmissible murine colonic hyperplasia. Infect. Immun. **61:**2486-2492.
36. **Sebesteny, A. and A. C. Hill.** 1974. Hepatitis and brain lesions due to mouse hepatitis virus accompanied by wasting in nude mice. Lab. Anim. **8:**317-326.
37. **Jiang, B., M. Jordana, Z. Xing, F. Smaill, D. Snider, R. Borojevic, D. Steele-Norwood, R. Hunt, and K. Croitoru.** 1999. Replication-defective adenovirus infection reduces *Helicobacter felis* colonization in the mouse in a gamma interferon- and interleukin-12 dependent manner. Infect. Immun. **67:**4539-4544.
38. **Schijns, V. E., B. L. Haagmans, C. M. Wierda, B. Kruithof, I. A. Heijnen, G. Alber, and M. C. Horzinek.** 1998. Mice lacking IL-12 develop polarized Th1 cells during viral infection. J. Immunol. **160:**3958-3964.
39. **Graham, M. B., D. K. Dalton, D. Giltinan, V. L. Braciale, T. A. Stewart, and T. J. Braciale.** 1993. Response to influenza infection in mice with a targeted disruption in the interferon gamma gene. J. Exp. Med. **178:**1725-1732.
40. **Parra, B., D. R. Hinton, N. W. Marten, C. C. Bergmann, M. T. Lin, C. S. Yang, and S. A. Stohlman.** 1999. IFN-gamma is required for viral clearance from central nervous system oligodendroglia. J. Immunol. **162:**1641-1647.